Conformational Flexibility of the Disaccharide α-D-Man*p*-(1→3)-*β*-D-Glc*p*-OMe Employing Molecular Dynamics Simulations and *trans*-Glycosidic $^3J_{C,H}$ from NMR Experiment

Christer Höög and Göran Widmalm*

Department of Organic Chemistry, Arrhenius Laboratory, Stockholm University, S-106 91 Stockholm, Sweden

Received: May 22, 2000; In Final Form: August 14, 2000

Molecular dynamics simulations of the disaccharide α-D-Man*p*-(1→3)-*β*-D-Glc*p*-OMe have been performed in vacuo and in water solution. Heteronuclear scalar coupling constants were measured across the glycosidic linkage. In conjunction with previously obtained experimental data, namely a *trans*-glycosidic proton−proton distance and the generalized order parameter a description of the molecular system is presented. The disaccharide exists in a major conformational state and has limited flexibility on a shorter time scale, i.e., less than its rotational correlation time (τ_M). Excursions to other conformational states are required to obtain agreement between simulation and experiment. Thus, on a longer time scale ($>\tau_M$) these conformational states are populated to some extent. The combined approach of molecular dynamics simulations and NMR experiments is therefore able to generate a consistent molecular picture.

Introduction

Carbohydrates, an important class of biomolecules, are commonly found in nature as polysaccharides or linked to other molecules, then known as glycoconjugates. The latter may be glycolipids, glycoproteins, or saponins. The biophysical characterization of these systems spans a wide range from rheological studies[1] to the investigation of atomic coordinate structure. Although several techniques are available, such as vibrational Raman optical activity,[2] optical rotation spectroscopy,[3] X-ray crystallography,[4] or noncontact atomic force microscopy,[5] and reveal important structural aspects, NMR spectroscopy is a technique of utmost importance being applied both in the solid and the liquid state.[6]

Several NMR parameters can be investigated leading to structural information. These are, for example, measurement of translational diffusion from which molecular size and hydration can be calculated.[7] The nuclear spin relaxation studies can reveal dynamics in the molecule.[8] Scalar coupling constants may be interpreted as a torsion angle and from the nuclear Overhauser effect distances within the molecule can be calculated. Recently, residual dipolar couplings have been shown to be important in structural refinement, in particular since they are sensitive to angular variation.[9] In many cases the NMR studies are combined with molecular modeling techniques since the experimental results can be interpreted in a molecular model describing the system in a three-dimensional way.[10]

In carbohydrates the glycosidic linkage plays a unique role. Stereochemical and conformational aspects have been studied in great detail and the most important have been named the anomeric effect and the *exo*-anomeric effect.[11] An understanding of the glycosidic linkage is essential in all aspects of oligo- and polysaccharides or derivatives thereof.

In the present study we extend our investigations on the disaccharide α-D-Man*p*-(1→3)-*β*-D-Glc*p*-OMe, similar in structure to disaccharide fragments found in bacterial polysaccharides or in glycoproteins, by performing CHARMM-based molecular dynamics (MD) simulations and measurement of *trans*-glycosidic heteronuclear scalar coupling constants. The results are combined with those previously obtained and a consistent picture of the conformational flexibility and the dynamics of the system is presented.

Materials and Methods

General. For the disaccharide α-D-Man*p*-(1→3)-*β*-D-Glc*p*-OMe (**1**) atoms in the glucosyl residue are denoted by *g*, and the mannosyl residue by *m*. The torsion angles at a glycosidic linkage are denoted by $\phi = $ H1*m*-C1*m*-O3*g*-C3*g* and $\psi = $ C1*m*-O3*g*-C3*g*-H3*g*.

NMR Spectroscopy. The NMR measurements of **1** (100 mM) were performed in D_2O:DMSO-d_6 at 30 °C on a Varian Inova 600 spectrometer. Measurements of *trans*-glycosidic $^1H,^{13}C$ coupling constants were performed using a ^1H detected gradient version with ^{13}C site selective excitation.[12,13] A spectral width of 1700 Hz was sampled with 16 384 complex points using 15 000 transients. A Hadamard two-site excitation, with a half-Gaussian pulse of 50 ms duration, was applied at the resonance frequencies of C1*m* and C3*g*. FIDs were processed using the VNMR software (Varian Associates). Zero-filling eight times and multiplication of the FID with an exponential weighting function with a line broadening factor of 0.3 Hz was applied prior to Fourier transformation. The *J*-doubling procedure used eight δ-functions in the frequency domain.[14]

Simulation. In all simulations the molecular mechanics program CHARMM[15] (parallel version, C25b2) was used with the CHARMM force field PARM22 (Molecular Simulations Inc., San Diego, CA), which is similar to the carbohydrate force field developed by Ha et al.[16] Simulations I−III were performed in vacuo and simulations IV and V were performed in aqueous solution. Initial conditions for simulations IV and V were prepared by placing the energy-minimized α-D-Man*p*-(1→3)-*β*-D-Glc*p*-OMe in a previously equilibrated cubic water box of length 29.972 Å containing 900 TIP3 water molecules, and removing those waters that were closer than 2.5 Å to any solute atom. This procedure resulted in a system with the disaccharide and 863 and 865 waters in simulations IV and V, respectively. Energy minimization was performed using Steepest Descent,

* Author to whom correspondence should be addressed.

10.1021/jp0018697 CCC: $19.00 © 2000 American Chemical Society
Published on Web 09/29/2000

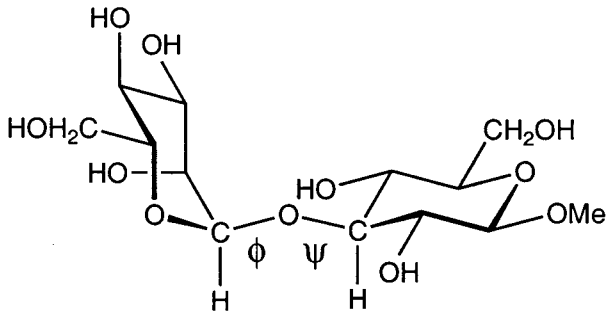

Figure 1. Schematic of α-D-Man*p*-(1→3)-*β*-D-Glc*p*-OMe (**1**) with the glycosidic torsion angles denoted by ϕ and ψ.

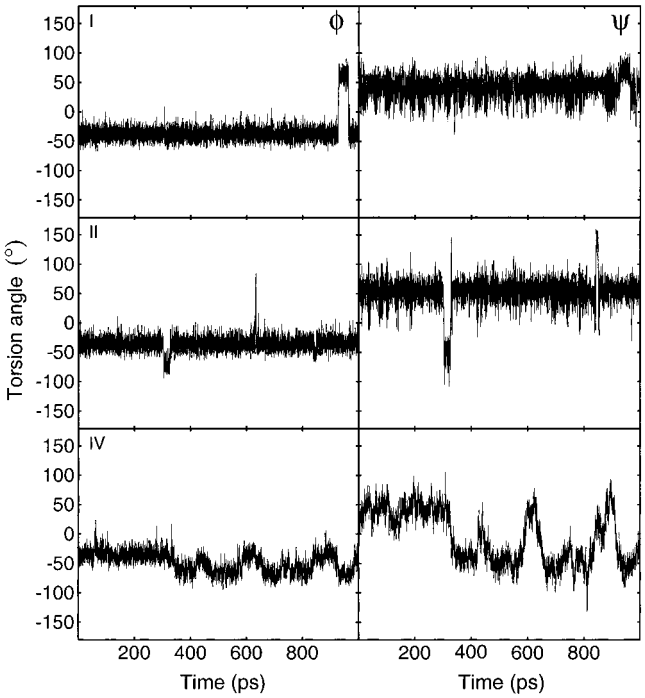

Figure 2. Molecular dynamics trajectories of **1** showing torsion angles ϕ (left column) and ψ (right column) from simulations I, II, and IV (top to bottom).

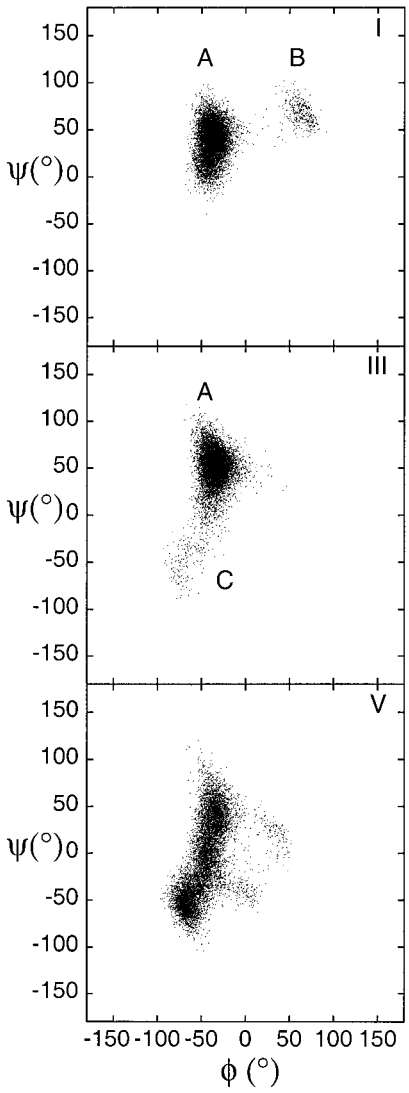

Figure 3. Scatter plots of ϕ vs ψ from the simulations I (top), III (middle), and V (bottom) of **1**. Conformational regions discussed in the text are marked as A, B, and C.

200 steps, followed by Adopted Basis Newton−Raphson until the root-mean-square gradient was less than 0.01 kcal mol^{-1} Å^{-1}. All MD simulations were started with assignment of initial velocities at 100 K followed by heating at 5 K increments during 4 ps to 300 K, where the systems were equilibrated for 100 ps. The production runs were performed for 1 ns. In simulations II−V the temperature was scaled by Berendsen's weak coupling algorithm.[17] Minimum image boundary conditions were used with a heuristic nonbond frequency update and a force shift cutoff acting to 12 Å. The simulations employed a dielectric constant of unity and a time step of 1 fs; data were saved every 0.1 ps for analysis. In simulations IV and V, SHAKE was used to restrain hydrogen-heavy-atom bonds,[18] with a tolerance gradient of 10^{-4}. The geometric criteria for hydrogen bonding was set to an oxygen−hydrogen distance <2.5 Å and a donor-hydrogen···acceptor angle Θ > 135°. Radial distribution functions (RDF) were integrated for oxygen−oxygen out to 3.5 Å and for hydrogen−oxygen to 2.5 Å to give the corresponding coordination numbers. The conformational states are averaged over the following time span: (A) 0−800 ps of simulation I, (B) 920−970 ps of simulation I, and (C) 305−325 ps of simulation II. All simulations were performed on an IBM SP2 computer at the Center for Parallel Computers, KTH, Stockholm. Simulations IV and V used 16 nodes resulting in a CPU time of approximately 4 h per 100 ps.

Results and Discussion

The disaccharide α-D-Man*p*-(1→3)-*β*-D-Glc*p*-OMe (Figure 1) was investigated by 5 MD simulations of 1 ns duration and are denoted as simulations I through V. In all simulations a CHARMM-based force field was used. Simulation I (in vacuo) presented in detail in this study is actually the CHARMM simulation referred to in our previous work[19] where it was used for comparison to other carbohydrate force fields, namely GLYCAM_93 and OPLS. In simulation I it should be noted that the transition that occurs around 900 ps (Figure 2) takes place for the ϕ torsion angle. The major conformational state in this simulation is denoted A, whereas the minor state is termed B (Figure 3). Flexibility at the ϕ torsion angle was observed in vacuo in our previous work. However, in all our previous simulations having explicit solvent molecules only single conformational states of limited flexibility were present. Simulations II (Figure 2) and III (Figure 3), also in vacuo, show transitions which are relatively small in magnitude for the ϕ torsion angle but large for the ψ torsion angle to a conformational region denoted C in this study. Essentially the same

TABLE 1: Results from MD Simulations and NMR Experiment

	ϕ (°)	$J\phi$ (Hz)[b]	$J\phi$ (Hz)[c]	ψ (°)	$J\psi$ (Hz)[b]	$J\psi$ (Hz)[c]	$r_{H1m,H3g}$ (Å)[d]	O2*g*−HO6*m* (%)[e]
simulation I	−34 [21][a]	3.5	3.9	40 [19]	3.3	3.7	2.29	50
simulation II	−36 [12]	3.7	4.2	50 [26]	2.4	2.6	2.35	32
simulation III	−35 [11]	3.8	4.3	50 [22]	2.4	2.5	2.34	34
simulation IV	−48 [17]	2.7	2.9	−6 [44]	3.3	3.7	2.49	28
simulation V	−46 [20]	2.8	3.0	−6 [42]	3.5	4.0	2.46	34
conformation A	−38 [9]	3.5	4.0	38 [18]	3.4	3.8	2.25	53
conformation B	63 [9]	1.5	1.4	69 [11]	1.2	1.0	3.24	0
conformation C	−70 [10]	1.1	0.9	−52 [17]	2.5	2.6	3.06	1
simulation W1[f]	−32 [9]	4.1	4.7	58 [10]	1.9	1.9	2.33	78
experiment		4.0			4.8		2.47[g]	

[a] Root-mean-square deviation in square brackets. [b] Calculated according to ref 25. [c] Calculated according to ref 26. [d] Calculated as $r = \langle r^{-3}\rangle^{-1/3}$. [e] Hydrogen bond from geometric criteria (see text). [f] Ref 19. [g] Ref 23.

TABLE 2: Hydrogen Bonds and Coordination Numbers from Simulation V

oxygen atom	acceptor	donor	total	n_{OO}	n_{OH}	n_{HO}	n_H
O1*g*	0.31		0.31	2.16	0.72		0.72
O2*g*	0.55	0.60	1.15	2.91	1.09	0.96	2.05
O3*g*	0.05		0.05	0.82	0.12		0.12
O4*g*	0.64	0.67	1.31	3.21	1.17	1.04	2.21
O5*g*	0.10		0.10	1.08	0.24		0.24
O6*g*	0.92	0.36	1.28	3.97	1.85	0.82	2.67
O2*m*	0.47	0.61	1.08	3.65	1.13	1.04	2.17
O3*m*	0.60	0.43	1.03	3.79	1.41	0.88	2.29
O4*m*	0.57	0.45	1.02	3.54	1.36	0.95	2.31
O5*m*	0.13		0.13	1.41	0.39		0.39
O6*m*	0.91	0.27	1.18	3.75	1.90	0.59	2.49

torsion angle averages are obtained for these two simulations (Table 1). Thus, flexibility in both torsion angles is revealed, which makes the system rather complex.

Influence of the solvent on the conformational preference has been noted.[20] Simulations IV and V were carried out with explicit water. The transitions of the torsion angles are slower than in vacuo. In simulation IV, essentially two states are present, A and C, and the ϕ/ψ transitions are correlated to each other (Figure 2). In particular, the larger flexibility at the ψ torsion angle is conspicuous. The results from simulation V (Figure 3) are similar to those from simulation IV. Torsion angle averages and root-mean-square deviations are summarized in Table 1. Inclusion of explicit water in the simulation shifts the average ϕ torsion angle slightly more negative, whereas the average ψ torsion angle is shifted to a larger extent (~60°) as a result of the increased population of conformational state C. Actually, in this case the conformational behavior is best described by an extended region comprising also the conformational states A and C defined above (see Figure 3). The lowering of torsional barriers in the presence of explicit water has previously been observed for glycol.[21] As in vacuo, the torsion angle averages in water are essentially the same after 1 ns of simulation.

The solute−solvent interaction can be studied by analysis hydrogen bonds and coordination numbers (Table 2).[22] The ring and bridge oxygens exhibit only low acceptor capabilities as is usually observed. The hydroxyl groups show about one hydrogen bond in total using both the distance and angle criteria. The lowest donor ability to solvent is observed for HO6*m*. The coordination numbers are obtained by integration of the radial distribution functions out to the first minimum. Of the hydroxyl groups n_{OO} and n_{OH} is lowest for O2*g* and whereas for n_{HO} the lowest value is present for HO6*m*. The total number of hydroxyl hydrogens involved in hydrogen bonds ($n_H = n_{OH} + n_{HO}$) is about twice as large as analyzed by pure hydrogen bond criteria. These results reveal a modified three-dimensional solvent structure in the region of the O2*g* and O6*m* groups. Analysis of the intramolecular hydrogen bond O2*g*−HO6*m* shows that this is present to ~30% in the simulations with explicit water (Table 1) and not just an artifact observed in the absence of water. The presence of an inter-residue hydrogen bond is consistent with our previous simulations.[19]

The dynamical behavior of **1** in the solvent mixture water: dimethyl sulfoxide (7:3) was studied by carbon-13 and proton nuclear spin relaxation which showed a *trans*-glycosidic distance between H1*m* and H3*g* of 2.45−2.48 Å.[23] Comparison between the solvent mixture and water on the conformation and *trans*-glycosidic distance revealed for some of the simulations that the averaged distance $r = 2.33$ Å (Table 1) was not changed between the solvents when the A conformational state was populated exclusively.[19] However, it was shorter than observed experimentally. Thus, the A conformer as described was not sufficient to explain experimental data. All three in vacuo simulations underestimate this *trans*-glycosidic distance but simulations IV and V with explicit water show an excellent agreement. Thus, population of either the B or the C conformational state or both to some extent result in a longer H1*m*−H3*g* distance, which is required (Table 1). The CHARMM-based force field which reveals a larger flexibility along the ψ torsion angle is in better agreement with experimental data than the force fields employed in our previous studies.

It is well-known that Karplus type relationships can describe torsion angles in molecules. Over the years several Karplus curves have been described, some addressing the *J* couplings over the glycosidic linkage in oligosaccharides. The general description of the Karplus type relationship is

$$^3J = A\cos^2\theta + B\cos\theta + C \qquad (1)$$

where θ is a torsion angle, *A*, *B*, and *C* are constants. A decade ago two Karplus curves were presented for glycosides by Mulloy et al.[24] and by Tvaroska et al.[25] which showed only minute differences in the constants. Most recently a modified equation was proposed by Cloran et al.[26] which is larger in magnitude. In the below analysis we used the two latter relationships.

The *trans*-glycosidic $^3J_{H,C}$ values were determined by selective excitation of carbon-13 resonances, followed by evolution of the long-range heteronuclear couplings, and detection of proton resonances employing two-site Hadamard spectroscopy. The $^3J_{H,C}$ values across the glycosidic linkage can be measured directly from the anti-phase separation in the resulting NMR spectrum (Figure 4), or extracted using the *J*-doubling procedure, which was employed in the present study. The resulting $^3J_{H,C}$ values are given in Table 1. As in our earlier work on different saccharides,[13] $J_\phi < J_\psi$. The compiled *J* values in Table 1 are most of the times underestimated from simulation using either Karplus curve. In the simulations with explicit water they are about 1 Hz too low. A shift of ~10° for the ϕ torsion angle to

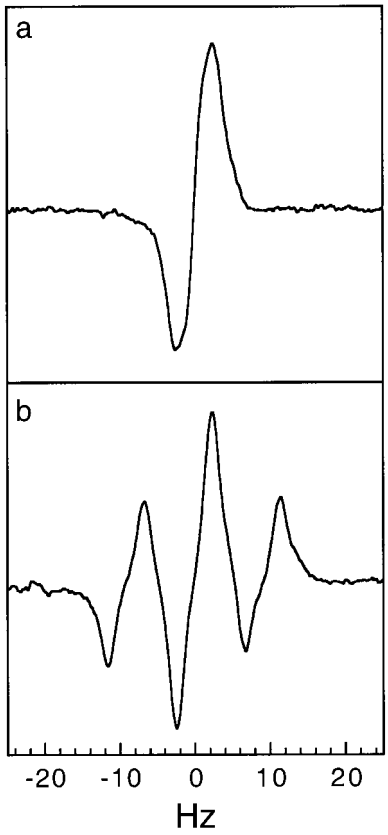

Figure 4. The resonances from (a) the anomeric proton H1′ of the mannosyl residue and (b) the proton H3 at the glycosyloxylated carbon of the glucosyl residue, after the long-range experiment with selective excitation of C3 and C1′, respectively. The anti-phase separation is equal to the *trans*-glycosidic $^3J_{H,C}$ values which were extracted by the *J*-doubling procedure.

that observed in vacuo (simulations I−III) results in good agreement for J_ϕ. However, that a large amount of conformation A is consistent with experimental data is obvious. Simulation W1 shows good agreement for ϕ but not at all for ψ. The approximately equal amount of A and C conformational states in water leads to a lower J_ψ value since conformation C has $\psi \approx -50°$. With respect to well A, a larger flexibility is required. Agreement between simulation and experiment can be obtained if the flexibility is extended toward the C well (which leads to a larger J_ψ value).

Glycosylation shifts in oligosaccharides may be used to study substitution positions, stereochemistry as well as conformational aspects.[27] The differences between chemical shifts in a disaccharide and those of the respective monomers are termed glycosylation shifts ($\Delta\delta$). For disaccharide **1** the magnitude of the carbon-13 displacements for both C1*m* and C3*g* at the glycosidic linkage upon glycosylation show $\Delta\delta_C \approx 6.6$ ppm.[28] As noted by Bock et al. there is an empirical relationship between carbon-13 glycosylation shift and the *trans*-glycosidic proton−proton distance.[29] Employing their equation ($-0.0776 \cdot \Delta\delta_C + 2.961$) the H1*m*−H3*g* distance is 2.45 Å, in excellent agreement with experimental data. The authors also discussed the ψ torsional angle dependence with respect to the glycosylation shift. However, we will not draw any conclusions from this, since it seems to be a function of the modulus of the torsion angle.[30]

The previous NMR study[23] also determined the Lipari−Szabo generalized order parameter (S^2) for **1** and it was found that $S^2 \approx 0.8$. We have calculated S^2 in conformation A from the simulations as the plateau of the reorientational correlation

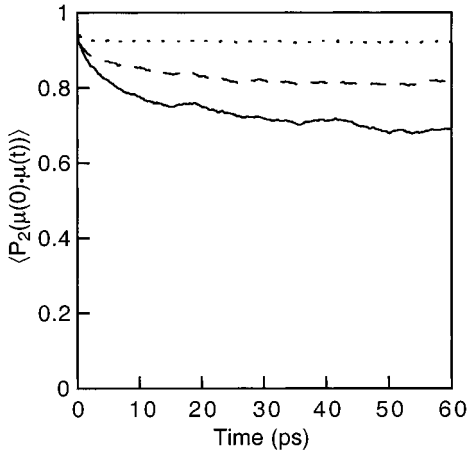

Figure 5. Reorientational correlation functions calculated for the CH vectors of C1*m*−H1*m* (solid line) and C5*m*−H5*m* (dashed line) and C5*g*−H5*g* (dotted line) form the first 300 ps of simulation IV (conformation A). These CH vectors show $S^2 \approx 0.7$, $S^2 \approx 0.8$, and $S^2 \approx 0.9$, respectively. The molecular reference frame was attached to the C2*m*−C5*m* and C2*m*−3*g* vectors.

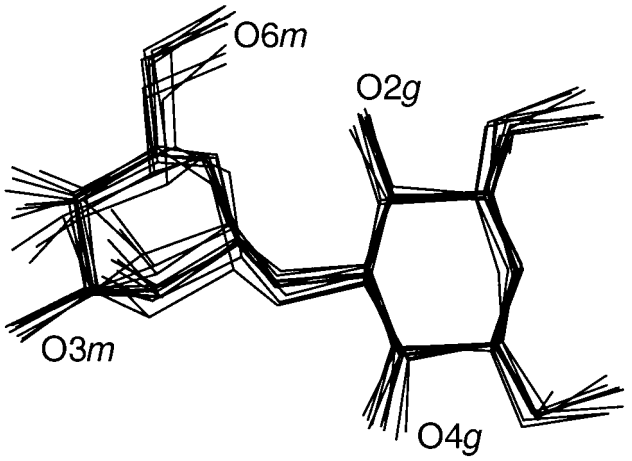

Figure 6. Overlay plot of **1**, based on the same molecular reference frame as in Figure 5, showing 10 structures during the first 300 ps of simulation IV. Selected oxygen atoms are annotated for ease of orientation.

function $\langle P_2(\mu(0)\cdot\mu(t))\rangle$ where the overall rotation has been removed. The results from representative CH vectors are presented in Figure 5 showing $S^2 \approx 0.7-0.9$. The description of α-D-Man*p*-(1→3)-β-D-Glc*p*-OMe having a single conformation of limited flexibility as shown by the 300 ps excerpt from the MD simulation with explicit water is in good agreement with earlier NMR studies as interpreted via S^2. Thus, this conformational behavior should be present on the order of the reorientational correlation time (τ_M) of the molecule. An overlay showing the conformational flexibility of state A is presented in Figure 6.

However, conformation A is not sufficient to explain experimental data and either of the conformations B or C leads to a longer *trans*-glycosidic distance H1*m*−H3*g*. On a longer time scale ($>\tau_M$) one or both of these conformations should be present. To improve the agreement for J_ψ, conformational excursions toward C-like conformers are necessary since simulated J_ψ values in conformation A are too low in comparison to experimental data.

Conclusions

The present study shows that MD simulation combined with several experimental results can be used to describe the behavior

and conformational flexibility at the glycosidic linkage in a disaccharide. The analysis and interpretation of results presented herein is not prone to generate virtual conformations, which may result when experimental data are used too heavily to restrain MD simulations. In the present case calculation from MD simulation of parameters deducible from NMR experiment, i.e., *trans*-glycosidic proton−proton distances, long-range heteronuclear coupling constants, and generalized order parameters lead to a straightforward comparison. The disaccharide can be described as having a major single conformation of limited flexibility on a shorter time scale ($< \tau_M$), but on a longer time scale ($> \tau_M$), excursions to one or two additional conformations are necessary to obtain agreement between simulation and experiment. Having a good understanding of the conformational region populated when two monosaccharides are linked together, structures of larger oligosaccharides can be addressed with greater credence.

Acknowledgment. This work was supported by a grant from the Swedish Natural Science Research Council.

References and Notes

(1) Yang, Z.; Huttunen, E.; Staaf, M.; Widmalm, G.; Tenhu, H. *Int. Dairy J.* **1999**, *9*, 631−638.
(2) Bell, A. F.; Hecht, L.; Barron, L. D. *J. Am. Chem. Soc.* **1994**, *116*, 5155−5161.
(3) Stephens, E. S. *Biopolymers* **1994**, *34*, 1403−1407.
(4) Eriksson, L.; Stenutz, R.; Widmalm, G. *Acta Crystallogr.* **1997**, *C53*, 1105−1107.
(5) McIntire, T. M.; Brant, D. A. *J. Am. Chem. Soc.* **1998**, *120*, 6909−6919.
(6) Ravindranathan, S.; Feng, X.; Karlsson, T.; Widmalm, G.; Levitt, M. H. *J. Am. Chem. Soc.* **2000**, *122*, 1102−1115.
(7) Rundlöf, T.; Venable, R. M.; Pastor, R. W.; Kowalewski, J.; Widmalm, G. *J. Am. Chem. Soc.* **1999**, *121*, 11847−11854.
(8) Palmer, A. G.; Williams, J.; McDermott, A. *J. Phys. Chem.* **1996**, *100*, 13293−13310.
(9) Landersjö, C.; Höög, C.; Maliniak, A.; Widmalm, G. *J. Phys. Chem. B* **2000**, *104*, 5618−5624.
(10) Asensio, J. L.; Cañada, F. J.; Cheng, X.; Khan, N.; Mootoo, D. R.; Jiménez-Barbero, J. *Chem. Eur. J.* **2000**, *6*, 1035−1041.
(11) *The Anomeric effect and associated stereoelectronic effects*; Thatcher, G. R. J., Ed.; American Chemical Society: Washington, DC, 1993.
(12) Nishida, T.; Widmalm, G.; Sándor, P. *Magn. Reson. Chem.* **1996**, *34*, 377−382.
(13) Rundlöf, T.; Kjellberg, A.; Damberg, C.; Nishida, T.; Widmalm, G. *Magn. Reson. Chem.* **1998**, *36*, 839−847.
(14) del Río-Portilla, F. D.; Blechta, V.; Freeman, R. *J. Magn. Reson. A* **1994**, *111*, 132−135.
(15) Brooks, B. R.; Bruccoleri, R. E.; Olafson, B. D.; States, D. J.; Swaminathan, S.; Karplus, M. *J. Comput. Chem.* **1983**, *4*, 187−217.
(16) Ha, S. N.; Giammona, A.; Field, M.; Brady, J. W. *Carbohydr. Res.* **1988**, *180*, 207−221.
(17) Berendsen, H. J. C.; Postma, J. P. M.; van Gunsteren, W. F.; DiNola, A.; Haak, J. R. *J. Chem. Phys.* **1984**, *81*, 3684−3690.
(18) Ryckaert, J. P.; Ciccotti, G.; Berendsen, H. J. C. *J. Comput. Phys.* **1977**, *23*, 327−341.
(19) Vishnyakov, A.; Widmalm, G.; Kowalewski, J.; Laaksonen, A. *J. Am. Chem. Soc.* **1999**, *121*, 5403−5412.
(20) Naidoo, K. J.; Brady, J. W. *J. Am. Chem. Soc.* **1999**, *121*, 2244−2252.
(21) Widmalm, G.; Pastor, R. W. *J. Chem. Soc., Faraday Trans.* **1992**, *88*, 1747−1754.
(22) Chandler, D. *Introduction to Modern Statistical Mechanics*; Oxford University Press: Oxford, 1987.
(23) Mäler, L.; Widmalm, G.; Kowalewski. J. *J. Phys. Chem.* **1996**, *100*, 17103−17110.
(24) Mulloy, B.; Frenkiel, T. A.; Davies, D. B. *Carbohydr. Res.* **1988**, *184*, 39−46.
(25) Tvaroska, I.; Hricovíni, M.; Petráková, E. *Carbohydr. Res.* **1989**, *189*, 359−362.
(26) Cloran, F.; Carmichael, I.; Serianni, A. S. *J. Am. Chem. Soc.* **1999**, *121*, 9843−9851.
(27) Söderman, P.; Jansson, P.-E.; Widmalm, G. *J. Chem. Soc., Perkin Trans. 2* **1998**, 639−648.
(28) Jansson, P.-E.; Kenne, L.; Persson, K.; Widmalm, G. *J. Chem. Soc., Perkin Trans. 1* **1990**, 591−598.
(29) Bock, K.; Brignole, A.; Sigurskjold, B. W. *J. Chem. Soc., Perkin Trans. 2* **1986**, 1711−1713.
(30) Gidley, M. J.; Bociek, S. M. *J. Am. Chem. Soc.* **1988**, *110*, 3820−3829.